INSTITUTO POTOSINO DE INVESTIGACIÓN CIENTÍFICA Y TECNOLÓGICA, A.C.

POSGRADO EN CIENCIAS APLICADAS

Characterization of Nanotubes and Fullerenes by the Pair Distribution Function

Tesis que presenta

Pedro Armando Ojeda May

Para obtener el grado de

Maestro en Ciencias Aplicadas

En la opción de

Nanociencias y Nanotecnología

Codirectores de la Tesis:

Dr. Mauricio Terrones Maldonado

Dr. Humberto Terrones Maldonado

San Luis Potosí, S.L.P., Abril de 2005.

IPICYT

Instituto Potosino de Investigación Científica y Tecnológica, A.C.

Acta de Examen de Grado

COPIA CERTIFICADA

El Secretario Académico del Instituto Potosino de Investigación Científica y Tecnológica, A.C., certifica que en el Acta 011 del Libro Primero de Actas de Exámenes de Grado del Programa de Maestría en Ciencias Aplicadas en la opción de Nanociencias y Nanotecnología está asentado lo siguiente:

En la ciudad de San Luis Potosí a los 4 días del mes de abril del año 2005, se reunió a las 18:00 horas en las instalaciones del Instituto Potosino de Investigación Científica y Tecnológica, A.C., el Jurado integrado por:

Dr. Humberto Terrones Maldonado	**Presidente**	**IPICYT**
Dr. Mauricio Terrones Maldonado	**Secretario**	**IPICYT**
Dr. Emilio Muñoz Sandoval	**Sinodal**	**IPICYT**
Dr. Ricardo Guirado López	**Sinodal externo**	**UASLP**

a fin de efectuar el examen, que para obtener el Grado de:

MAESTRO EN CIENCIAS APLICADAS
EN LA OPCIÓN DE NANOCIENCIAS Y NANOTECNOLOGÍA

sustentó el C.

Pedro Armando Ojeda May

sobre la Tesis intitulada:

Characterization of Nanotubes and Fullerenes by the Pair Distribution Function

que se desarrolló bajo la dirección de

Dr. Humberto Terrones Maldonado
Dr. Mauricio Terrones Maldonado

El Jurado, después de deliberar, determinó

APROBARLO

Dándose por terminado el acto a las 20:15 horas, procediendo a la firma del Acta los integrantes del Jurado. Dando fé el Secretario Académico del Instituto.

A petición del interesado y para los fines que al mismo convengan, se extiende el presente documento en la ciudad de San Luis Potosí, S.L.P., México, a los 4 días del mes abril de 2005.

Dr. Marcial Bonilla Marín
Secretario Académico

INSTITUTO POTOSINO DE INVESTIGACIÓN CIENTÍFICA Y TECNOLÓGICA, A.C.
IPICYT
SECRETARIA ACADEMICA

Mtra. Ma. Elisa Lucio Aguilar
Jefa del Departamento de Asuntos Escolares

INSTITUTO POTOSINO DE INVESTIGACION CIENTIFICA Y TECNOLOGICA, A. C.

DIVISION DE MATERIALES AVANZADOS PARA LA TECNOLOGIA MODERNA

MAESTRIA EN NANOCIENCIAS Y NANOTECNOLOGIA

CHARACTERIZATION OF NANOTUBES AND FULLERENES THROUGH THE PAIR DISTRIBUTION FUNCTION

Ing. Fís. Pedro Armando Ojeda May

SINODALES

Dr. Humberto Terrones Maldonado
(Asesor de tesis)

Dr. Mauricio Terrones Maldonado
(Asesor de tesis)

Dr. Emilio Muñoz Sandoval

Dr. Ricardo Guirado López

Contents

Chapter 1

Introduction

Contents

The discovery of fullerenes and identification of carbon nanotubes by Kroto [1] and Iijima [2] respectively initiated a new field in Physics, Chemistry and Materials Science. At present, fullerenes and carbon nanotubes can be produced using various techniques: arc-discharge [3], pyrolisis of hydrocarbons over catalysts [4], laser [5], solar vaporisation [6], and electrolysis [7].

The progress in this field has been exceptional, however there are still unsolved questions regarding carbon nanostructures about their electronic structure, growth mechanisms, chirality determination, doping, etc.

1.1 Chirality

In this work we focus on the questions about the chirality determination of carbon nanotubes, the presence of geometrical imperfections such as pentagons and heptagons and the growth mechanism using carbon dimers addition. As we know from chemistry, a chiral molecule is one that is not superimposable on its mirror image; it has the property of rotating the plane of polarisation of plane-polarised monochromatic light that is passed through it (optical activity). In the context of carbon nanotubes, chirality (helicity) is a term employed to denote the way in which a graphene sheet rolls up to form a tube. Depending on the chirality of the nanotube, we can obtain a semiconductor, metal or insulator structure. This feature is very important for many effects found in carbon nanotubes such as the 1D-Luttinger liquid where all of the nanotubes taking a role in this effect are metallic nanotubes [8].

The chirality of individual single- and multi-walled nanotubes and bundles of them [9] has been characterized in the past by a variety of methods, such as nanodiffraction [10], high resolution Raman spectroscopy [11, 12], scanning tunneling microscopy (STM) [13] and infrarred spectroscopy (IR) [14]. However, these techniques are local, in the sense that they focus on specific regions of the volume of the sample. In order to study structures on a bulk scale, we need different techniques such as neutron diffraction and/or X-ray powder diffraction. Both of them allow to calculate the Pair Distribution Function (PDF), which provides information about the most common distances between atoms in the nanostructures.

It has been revealed that there are several diameters and different chiralities within one single sample [13, 15]. Fig 1.1 shows STM images of individual

tubes in a bundle that are located at the surface of the bundle. All these tubes were of different chiralities. As we have mentioned above, at present, the main challenge in nanotube science is to produce SWNTs with specified diameter and one chirality, in a selective way, so that these could be used in the fabrication of nanoelectronic devices.

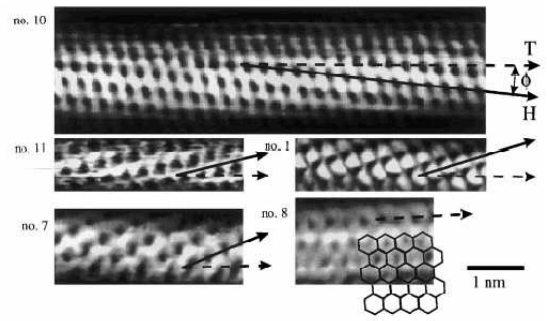

Figure 1.1: Images of SWNTs showing that in a bundle, we can observe different chiralities. Image taken from Ref. [13].

On the other hand, certain methods produce nanotubes with preferred chiralities; high resolution transmission electron microscopy (HRTEM) images have provided experimental evidence of this fact [10, 16, 17, 18]. In Fig 1.2 is shown a bundle cross-section of SWNTs, mainly armchairs of approximately 1.4 Å in diameter. In the cases where the sample contains almost all of the nanotubes of the same chirality, as it was demonstrated by using X-ray diffraction and transmission electron microscopy (TEM) [18], we are not interested in the diffraction of individual nanotubes. Instead, we would require a technique that could be used to obtain the average chirality without measuring the chirality of nanotubes and then obtaining the average.

In this work we propose to determine the chirality of nanotubes in the bulk using the pair distribution function (PDF) obtained from neutron diffraction experiments. It is interesting to notice that PDF works in real space whereas diffraction measurements work in reciprocal space. A typical PDF pattern shows the most common distances found in a molecule or cluster as well as their size. The distances can be obtained from the structures by identifying the peaks of the PDF, and the structure sizes are obtained from the comparison of the decay of the signals with the most intense peaks.

A particular feature of the PDF technique is that it takes into account

only average distances and not the particular environment of an atom. Thus, within this technique we take into account a sort of average chiralities of a bulk sample.

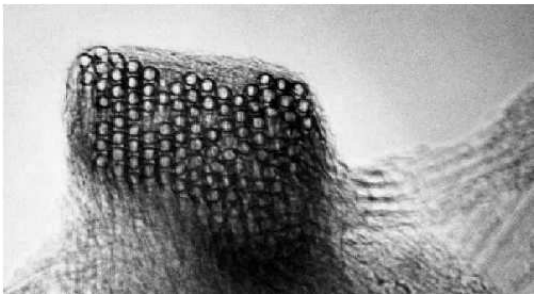

Figure 1.2: Certain methods can produce nanotubes with a preferred chirality. The bundle cross-section shown in this figure, Ref. [17], consists mainly of armchair nanotubes with an average diameter of 1.4 Å, packed in a hexagonal crystalline way.

Because carbon atoms in a carbon nanotube possess a particular arrangement depending on their chirality, it is clear that the C-C distances will be different for each other. Actually, it is expected to have different PDF patterns for each nanotube. We think that this technique could help us to determine the nanotube chirality of different samples. Up to now, we have worked with armchair and zigzag nanotubes. These nanotubes have characteristic distances and we can distinguish them theoretically. Chiral nanotubes are the next step.

We also studied other carbon nanostructures such as Haeckelites and Fullerenes. Haeckelites are a new form of nanotubes in which heptagon-pentagon defects are introduced in the lattice. Hackelites were predicted theoretically and were found to be more stable than fullerenes [19]. We studied the PDF in the case of Haeckelites and found that it is possible to distinguish them from conventional SWNTs (just hexagons in the lattice). For Fullerenes, we found that distances related to pentagonal defects disappear when the diameter of the fullerene is increased and that the distances change with respect to smaller fullerenes.

The outline of this thesis is as follows. In Chapter 2, we discuss the two most common techniques used to characterize SWNTs chiralities. We propose another technique based on neutron diffraction method which allows us to obtain the PDF of a sample. In Chapter 3, we present our results of

the PDFs of armchair and zigzag nanotubes, and compared them with experimentally obtained PDF, of a sample of nanotubes prepared using High Pressure of CO (HIPCo) process. Finally, in Chapter 4, we write our discussions, conclusions and future work.

Bibliography

[1] *C60: Buckminsterfullerene*, H. W. Kroto, J. R. Heath, S. C. O'Brien, R. F Curl and R. E. Smalley, Nature (London) **318**, 162, (1985).

[2] *Helical microtubules of graphitic carbon*, S. Iijima, Nature (London) **354**, 56 (1991).

[3] *Carbon nanotubes in cathodic vacuum arc discharge*, Takikawa H., Yatsuki M., Sakakibara T., and Itoh S., J. Phys. D **33**, 826 (2000).

[4] *Organimetallic precursor route to carbon nanotubes*, Govindaraj A. and Rao C. N., Pure Appl. Chem. **74**, 1571 (2002).

[5] *Large-scale synthesis of carbon nanotubes*, Ebbesen T. and Ajayan P. M., Pure Appl. Chem. **74**, 1571 (2002).

[6] *Carbon nanotubes: dynamics of synthesis processes.* Laplaze D., Alvarez L., Guillard T., Badie J. and Flamant G., Carbon **40**, 1621 (2002).

[7] *Carbon Nanotubes: Synthesis, Structure, Properties and Applications*, Dresselhaus, M. S., G. Dresselhaus and Ph. Avouris, (Springer-Verlag, Heidelberg, Germany, 2001).

[8] *Scanned probe microscopy of electronic transport in carbon nanotubes*, Bachtold, A., M. S. Fuhrer, S. Plyasunov, M. Forero, E. H. Anderson, A. Zettl, and P. L. McEuen, Phys. Rev. Lett. **84**, 6082 (1994).

[9] *Resonant Raman spectra for isolated single-wall carbon nanotubes grown*, A. Jorio, R. Saito, J. H. Hafner, C. M. Lieber, M. Hunter, T. McClure, G. Dresselhaus and M. Dresselhaus, Phys. Rev. Lett. **86**, 1118 (2001).

[10] *Boron-mediated growth of long helicity-selected carbon nanotubes*, X. Blase, J. C. Charlier, A. De Vita, R. Car, Ph. Redlich, M. Terrones, W. K. Hsu, H. Terrones, D. L. Carroll and P. M. Ajayan, Phys. Rev. Lett. **83**, 5078 (1999).

[11] *Chirality-dependent G-band Raman intensity of carbon nanotubes*, R. Saito, A. Jorio, J. H. Hafner, C. M. Lieber, M. Hunter, T. McClure, G. Dresselhaus and M. Dresselhaus, Phys. Rev. B **64**, 085312 (2001).

[12] *Observations of the D-band feature in the Raman spectra of carbon nanotubes*, S. D. M. Brown, A. Jorio, G. Dresselhaus and M. Dresselhaus, Phys. Rev. B **64**, 073403-1 (2001).

[13] *Electronic structure of atomically resolved carbon nanotubes*, J. W. Wildöer, L. Venema, A. G. Rinzler, R. Smalley and C. Dekker, Nature (London) **391**, 59 (1998).

[14] *Spectroscopic study of the Fermi level electronic structure of single-walled carbon nanotubes*, Itkis M., Niyogi S., Meng M., Hamon M., Hu H., and Haddon R., Nano Letters **2**, 155 (2002).

[15] *Atomic structure and electronic properties of single-walled carbon nanotubes*, T. Odom, J.-L. Huang, P. Kim, C. M. Lieber, Nature (London) **391**, 62 (1998).

[16] *Structure of carbon nanotubes probed by local and global probes*, Ph. Lambin, A. Loiseau, C. Culot and L. P. Biró, Carbon **40**, 1635 (2002).

[17] *Crystalline ropes of metallic carbon nanotubes*, A. Thess, R. Lee, P. Nikolaev, H. Dai, P. Petit, J. Robert, C. Xu, Y. H. Lee, S. G. Kim, A. G. Rinzler, D. Colbert, G. Scuseria, D. Tománek, J. E. Fischer and R. Smalley, Science **273**, 483 (1996).

[18] *Metallic resistivity in cristalline ropes of single-wall carbon nanotubes*, J. E. Fisher, H. Dai, A. Thess, R. Lee, N. M. Hanjani, D. L. Dehaas, and R. E. Smalley, Phys. Rev. B **55**, 4921 (1997).

[19] *New metallic allotropes of planar and tubular carbon*, H. Terrones, M. Terrones, E. Hernández, N. Grobert, J-C. Charlier and P. M. Ajayan Phys. Rev. Lett. **84**, 1716 (2000).

[20] *An Atlas of Fullerenes* , P. W. Fowler and D. E. Manolopoulos, (Clarendon Press, Oxford, 1995).

[21] *Fullerene growth and the role of non-classical isomers*, E. Hernandez, P. Ordejon, and H. Terrones, Phys. Rev. B **63**, 193403 (2001).

[22] *New empirical model for the structural properties of silicon*, Phys. Rev. B **56**, 632(1986).

[23] *Nobel Lectures, Chemistry 1996-2000*, Ingmar Grenthe, (World Scientific Publishing Co., Singapore, 2003).

[24] *Characterizing carbon nanotube samples with resonance Raman scattering*, A. Jorio, M. A. Pimenta, A. G. Souza Filho, R. Saito, G. Dresselhaus and M. S. Dresselhaus, New Journal of Physics **5**, 139.1 (2003).

[25] *Chirality effect of single-wall carbon nanotubes on field emission*, S.-D. Liang and N. S. Xu, Appl. Phys. Lett. **83**, 1213 (2003).

[26] *Second-order resonant Raman spectra of single-walled carbon nanotubes*, S. D. M. Brown, P. Corio, A. Marucci, M. A. Pimenta, M. S. Dresselhaus and G. Dresselhaus, Phys. Rev. B **61**, 7734 (2000).

Chapter 2

Techniques to characterize carbon nanotubes

Contents

Exploring the applications of carbon nanostructures in a reliable way requires a sample characterization as precise as possible. In this context, we could use Raman spectroscopy and all sorts of diffraction techniques. In particular, Raman scattering is widely used to investigate both vibrational and electronic properties of solids. In the case of SWNTs, the diameter and chirality can be obtained by studying the modes measured in Raman spectroscopy, among which the most relevant are the G-mode and the radial breathing mode (RBM). On the other hand, the diffraction techniques comprise the electron diffraction, the neutron diffraction, and the X-ray diffraction. They are esentially based on the Fourier transform of an structure. It is the diffraction pattern that lies in the reciprocal space and provides information, by means of a set points, about the chirality of the nanotubes. SWNTs are generally arranged in ropes, that should be characterized as well. It is well established that the nanotubes in a rope could exhibit different chiralities and their diameters also can vary. With a transmission electron microscope or a scanning probe microscope, it is possible to examine the individual tubes in a rope. However, it might prove advantageous to obtain more global information on the rope. At a larger scale, the ropes themselves form entangled networks for which averaged structural data are required. These can be obtained by X-ray or neutron diffraction, and by Raman spectroscopy. Structural characterization of nanotubes is also essential to understand the growth mechanisms, to study the influence of the synthesis conditions, or to analyze the efficiency of a purification process.

2.1 Raman spectroscopy

Raman literature about chemical applications appears after 1986 while almost all of the theoretical work was carried out earlier [1]. This chronological fact was due to technical issues, including weak intensity, flourescence interference, and inefficient light collection and detection. This fact changed in 1986 with the introduction of Fourier transform (FT) Raman technique, small computers and near-infrared lasers. The Raman scattering is explained as a superposition between optical and vibrational oscillations in the electron cloud of a molecule (dipole of the molecule classically). These oscillations arise when a monochromatic light of energy $h\nu_o$ encounters matter (gas, solid, or liquid) and there is a small probability that it will be scattered at the same frequency. However, a small fraction of light (approximatelly 1

photon in 10^7) is scattered at optical frequencies different from, and usually lower than, the frequency of the incident photons. The process leading to this inelastic scattering is known as the Raman effect. Raman scattering could occur with a change in vibrational, rotational or electronic energy of a molecule. Chemists are concerned primarily with the vibrational Raman effect. The difference between the incident photon and the Raman scattered photon is equal to the energy of a vibration quanta of the scattering molecule. A Raman spectrum consists of scattered intensity plotted vs. energy (or frequency), as shown in Fig 2.1. Each peak corresponds to a given Raman shift from the incident light energy $h\nu_o$. From the quantum mechanical point of view, the interaction is seen as an excitation to a virtual state lower in energy than a real electronic transition with nearly coincident de-excitation and a change in vibrational energy. The energy difference between the incident and scattered photons is represented by the arrows of different lengths in Fig 2.2. The vibrational energy is dissipated as heat, but, because of the low energy of the Raman scattering the sample is not heated appreciably. When the

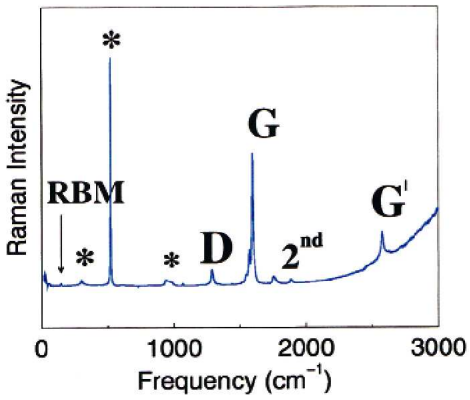

Figure 2.1: Raman spectrum from one nanotube taken over a broad frequency range using E_{laser} = 785 nm excitation and showing the radial breathing mode (RBM), the D-band, the G-band and the G'-band. Second-order modes are also observed. The features marked with an asterisk (*) at 303, 521, and 963 cm^{-1} are from the Si/SiO_2 substrate and are used for the calibration of the nanotube Raman spectrum [2].

initial population of excited states is approximatelly zero (but not exactly zero), the initial state can be considered as the ground state and the scattered photon will have lower energy than the incident photon. This effect

is called Raman Stokes scattering depicted in Fig. 2.2. In the real world, there always exist a certain number of excited states in a molecule. Raman scattering from vibrationally excited molecules leaves the molecule in the ground state. The scattered photon appears at higher energy, as shown in Fig. 2.2. This anti-Stokes shifted Raman sprectrum is always weaker than the Stokes-shifted spectrum, but at room temperature it is strong enough to be useful for vibrational frequencies less than about 1500 cm^{-1}. The Stokes and anti-Stokes spectra contain the same frequency information.

The Raman spectrum is characterized for 16 modes. In the next subsections, we will briefly discuss three kinds of modes and the information that can be extracted from them in the frame of carbon nanotube spectroscopy.

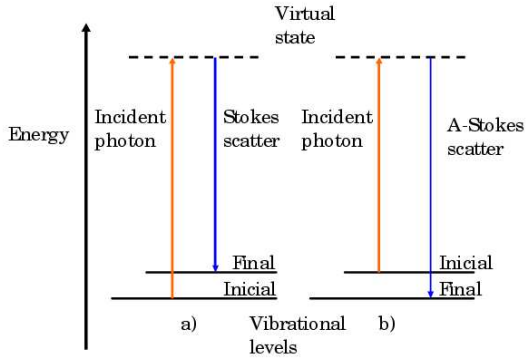

Figure 2.2: Raman scattering is divided into two types that are known as Stokes and anti-Stokes scattering. In the first case, the Stokes scatterer is lower in energy than the incident photon while in the latter the anti-Stokes scatterer is higher in energy than the incident photon. These two processes give equivalent information about the sample.

2.1.1 Radial breathing mode (RBM)

The Raman features (appearing between 120 $cm^{-1} < \omega_{RBM} < 250$ cm^{-1} for SWNTs within 1 nm $< d_t <$ 2 nm diameters) correspond to the atomic vibration of the C atoms in the radial direction, as if the tube was breathing

(Fig. 2.3). These features are very useful for characterizing nanotube diameters through the relation $\omega_{RBM} = A/d_t + B$, where the parameters A and B are determined experimentally. For typical SWNT bundles in the diameter range $d_t = 1.5 \pm 0.2$ nm, the values $A = 243$ cm^{-1} nm and $B = 10$ cm^{-1} has been found for SWNTs bundles (where B is an upshift coming from the tube-tube interaction). For isolated SWNTs on an oxidized Si substrate, $A = 248$ cm^{-1} nm and $B = 0$ have been found. It is important to point out that, for the usual diameter range 1 nm $< d_t <$ 2 nm, these two sets of parameters provide similar d_t for a given ω_{RBM}, differing considerably only for $d_t <$ 1 nm and $d_t >$ 2 nm. However, for $d_t <$ 1 nm, the simple $\omega_{RBM} = A/d_t + B$ relation is not expected to hold due to nanotube lattice distortions leading to a chirality dependence of ω_{RBM}. For large diameter tubes ($d_t >$ 2 nm) the intensity of the RBM feature is weak and is hardly observable. It is also

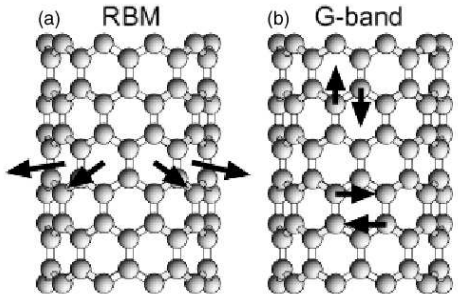

Figure 2.3: Two possible modes of the Raman vibrational spectrum. (a) Radial breathing mode (RBM modes), (b) Tangential modes (G mode) [3].

important to mention the role of the laser energy. At any energy, it is possible to excite the molecules, however the intensity of the Raman spectrum could be weak. When we use a laser energy close to energies with a very high population of quantum states, known as Van Hove singularities in the density of states, we obtain a clear Raman spectrum (higher intensity) the so called Raman resonance scattering. In Fig. 2.4 the densities of states for three SWNTs calculated by means of tight-binding method are displayed and the corresponding Raman spectrum. For this case, it is plotted the diamater of the nanotube vs. the difference of energy between the first two Van Hove singularities labeled as E_{ii}^s. Those maps are known as Kataura plots, see for further details [4].

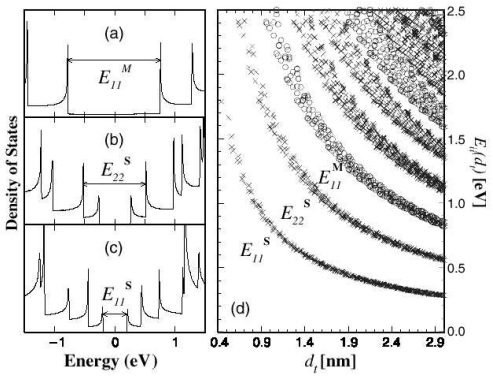

Figure 2.4: Density of states for three SWNTs calculated using tight-binding method showing the Van Hove singularities. As we can see, the energy difference between symmetrical peaks, labeled as E_{ii}^{s}, is characteristic of each nanotube, therefore it can be used as a fingerprint. By using Raman scattering, these energy differences are plotted vs. the diameter of the nanotube in maps called Kataura plots. Important information can be extracted from these maps, such as the diameter of the nanotube and the chirality [3].

2.1.2 Tangential modes - G band

The observation of characteristic multiple peak features around 1580 cm^{-1} also provides a signature of carbon nanotubes. Spectra in this frequency range can be used for SWNTs characterization, independent of the RBM observation. This multiple peak feature can, for example, also be used for diameter characterization, although the information provided is less accurate than the RBM feature, and it provides information about the metallic character of the SWNTs in resonance with a given laser line. The G modes of vibration are shown in Fig. 2.3.

The Raman-allowed tangential mode in graphite is observed at 1582 cm^{-1}, and is called the G mode (from graphite). The tangential G mode in SWNTs gives rise to a multi-peak feature, also named G band, where up to six Raman peaks can be observed in a first-order Raman process. However, a simple analysis can be carried out considering the most intense G peaks that are labeled as G^{+}, for atomic displacements along the tube axis, and as G^{-}, for modes with atomic displacement along the circumferential direction. The lowering of the frequency for the G^{-} mode is caused by the curvature of the nanotube which softens the tangential vibration in the circumferential

direction. The difference between the G band lineshape for semiconducting and metallic SWNTs is evident in the lineshape of the G^- feature, which is broadened for metallic SWNTs in comparison with the Lorentzian lineshape for semiconducting tubes. This broadening is related to the presence of free electrons in nanotubes with metallic character.

2.1.3 Disorder-induced modes - D band

Nowadays, it is believed that the disorder band (D band) could be helpful to characterize many deffects in carbon nanotubes, such as, vacancies, kinks, heptagon-pentagon pairs; however the question is still open. In some cases the G band is more intense than the D band indicating certain order in the sample, however when the reverse is true we guarantee the presence of amorphous carbon, because of the bad resonance condition. In these cases, the observation of a peak around 1450 cm^{-1} is also common. The RBM, the G-band and the D-band are shown in Fig. 2.1.

2.2 Electron diffraction

The nanotubes were identified using High Resolution Transmission Electron Microscopy (HRTEM) combined with electron diffraction, that also allowed to investigate the chiralities of a nanotube. The images of the HRTEM consist of projections along the propagation direction of the electron beam. The information that can be extracted from these techniques accounts for: (i) self-organization of the tubes and the density of tubes (approximately), (ii) diameters of the tubes, and (iii) atom distribution (helicity) of the tubes. Carbon nanotubes could be assembled in a nested configuration (multiwall nanotubes) or as single ropes. Images obtained from HRTEM allow us to meassure the diameters of the nanotubes and their thickness whithin a certain uncertainty range, which also depends on the orientation of the electron beam with respect to the axis parallel to the nanotube direction as shown in Fig. 2.6 (a). Depending on the resolution power of the electron microscope, we can observe bundles of nanotubes [Fig. 2.6 (b)] or the fringes of the carbon nanotubes [Fig. 2.6 (c)], parallel lines shown as a shade region in Fig. 2.5 (a), which are important to identify deffects as kinks and catalyst impurities. It is a common practice to observe multiwall nanotubes in the perpendicular direction to the electron beam, because in this way, it is possible to obtain

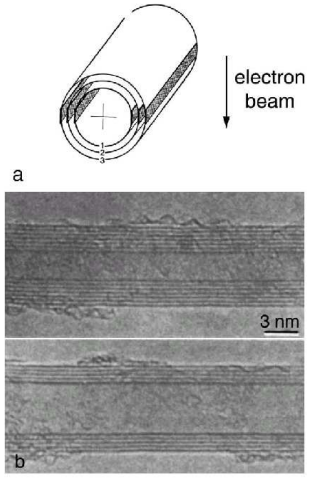

Figure 2.5: (a) An electron beam in the perpendicular direction of the tube axis is incident. (b) The HRTEM images show that fringes, parallel lines, arise as a consequence of the stacked honeycomb layered structure which permits to calculate the diameter of the tube directly [5].

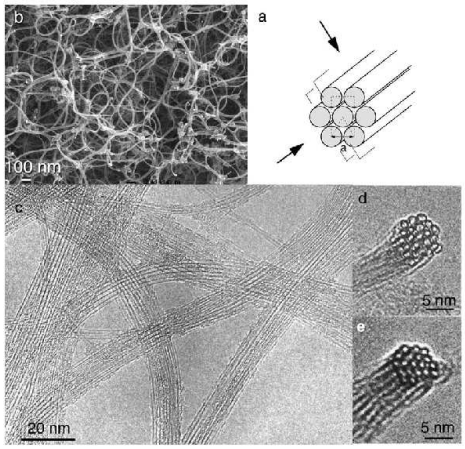

Figure 2.6: (a) Model of a nanotube rope with different electron beam directions; (b) Scanning electron micrograph of SWNTs ropes; (c) HRTEM images at different magnifications showing the whole bundle or a single tube; (d)-(e) cross-section of SWNTs ropes [3].

the number of nanotube walls and therefore the diameter of the tube.

2.2.1 Chiralities of the carbon nanotubes

If we want to use HRTEM images to distinguish the atomic arrangement of carbon atoms in a SWNT, we would need a resolution better than 0.2 nm. Otherwise, we would observe only the bundle continuos or a section of the tube. The first atomic images have been obtained by scanning tunneling microscopy (STM). This method consists in measuring the differential conductance (related to the density of states) and plotting this in a 3-D map for each spatial point. In this way, we get a contour plot of a certain surface. This method is very local, in the sense that we can observe only a small part of a surface. It is also restricted to individual single layer nanotubes and does not allow the analysis of a large number of objects. Transmission Electron Microscopy (TEM) images (Figs. 2.5-2.6) do not provide any information on the helicities of the nanotubes. In order to identify the nanotube chirality, it is necessary to obtain direct images of the atomic positions for each tube. However, we have to overcome two difficulties. Firstly, the spatial resolution of the microscope. Secondly, the unavoidable observation in projection makes difficult the identification of the atomic positions of several self-assembled layers. Fortunatelly, this problem was solved with the use of the electron diffraction technique. In this case we obtain a pattern of intensities in the reciprocal space independent of the number of layers and related to the scattering section of the sample. We need to emphasize that a reduced number of layers in a nanotube produces weak scattering intensities, and therefore the intensity patterns for SWNTs are less common than those observed for MWNTs.

2.2.2 Electron diffraction

The atomic structure of individual carbon nanotubes has mostly been investigated by selected-area diffraction in TEM. Nanodiffraction has been used too, but almost exclusively for the study of ropes of SWNTs [6, 8].

In the electron diffraction pattern of a nanotube, the intensities are localized along lines perpendicular to the nanotube axis. Along each line, the intensity is modulated. This modulation is due to the finite width (the diameter) of the nanotube. For a single-wall chiral nanotube, 12 spots with larger intensities are distributed around the vertices of two hexagons inscribed in

the first diffraction circle. In Fig.2.7, we present the theoretical diffraction patterns calculated using EMS software for three kinds of nanotubes, see [3] for further details. The chiral nanotube (17,4) shown in the central part [Fig.2.7 (c)] displays the spots around the first diffraction circle which come from the (100) nodes generated by the honeycomb structure. Outside, there is another circle formed by (110) spots. All the graphene reflections of the type ($hk0$) are elongated in the direction normal to the tube axis (size effect). The splitting of the (100) spots on two hexagons originates from the

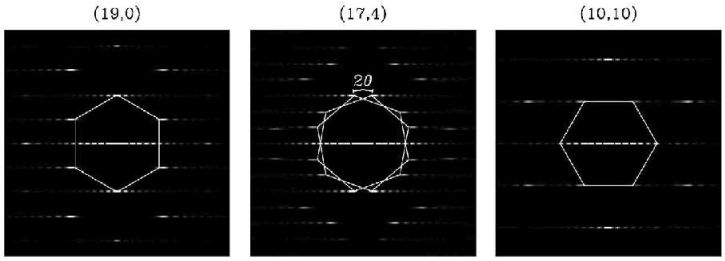

Figure 2.7: Theoretical electron diffraction patterns for three SWNTs. (a) and (c) correspond to non-chiral (19,0) and (10,10) nanotubes, respectively. (b) A chiral (17,4) nanotube. The chiral angle of the nanotube can be determined from the rotation angle between the two hexagons formed by the diffraction peaks [3].

two halves of the nanotube located on both sides of the plane through the axis perpendicular to the electron beam front and back (the electron beam is assumed to be perpendicular to the axis). The projection in this plane of the atomic structure of the two nanotubes halves are rotated from each other by twice the chiral angle. The diffraction patterns they produce are rotated by the same angle, which means that the angle between the two hexagons in the first diffraction circle is two times the chiral angle of the nanotube. The helicity of the atomic structure of a nanotube can therefore be measured directly in the diffraction pattern, as illustrated in Fig 2.7. When the electron beam is not perpendicular to the tube axis, a correction must be applied to the observed angular splitting of the (100) spots. For non-chiral nanotubes, either zig-zag or armchair, the two hexagons in the first diffraction circle coincide.

Most of the experimental studies of individual nanotubes by electron diffraction have been realized on multiwall systems. On rare occasions, isolated SWNTs have been investigated by this technique. This is because, when

by chance an SWNT is isolated, it produces little intensities. The diffraction pattern of an MWNT is close to a superimposition of the patterns produced by the individual layers. In principle, the amplitudes of the wave diffracted by the layers add coherently, and not the intensities. But the interferences between the diffracted waves mostly result in a strong modulation of intensity along the equatorial line only, with a period $2\pi/c_o$ related to the interlayer spacing c_o (around 3.4 Å), generating thereby the graphite like (002l) spots. The (100) spots around the first diffraction circle are distributed according to the different helicities. From this distribution, it appears that the MWNTs are in general polychiral.

2.2.3 X-ray and neutron diffraction

With X-rays and neutrons, many nanotubes are probed with, in general, all possible orientations with respect to the incident direction. This means that the power-like diffraction profiles are obtained, where the intensity is recorded versus the modulus of the scattering wave vector q or, equivalently, the scattering angle 2θ. The nanotubes in the sample have different diameters and chiralities, and they may have different number of layers. As a result of these variations, only a statistical characterization of the sample can be obtained.

For multiwall carbon nanotubes, a diffraction profile is composed of two families of peaks. The graphite-like (002l) peaks occur at integer multiples of $2\pi/c_o$. Their positions give information on the spacing c_o between the layers (c_o around 3.4 Å). These peaks are nearly symmetric in shape. The slight asymmetry is caused by a continuous decrease of the interlayer distance (size effect). The intensity and width of these peaks depend on the number of layers, on the variations of the interlayer spacings and on lattice distortions. The second family of peaks is due to the honeycomb structure of the individual layer and comprises the (kh0) reflections of a graphite sheet.

Neutrons have the advantage over the X-rays that the atomic factor $f(q)$ does not decrease with q, in fact it is a constant independent of q. A diffraction profile can therefore be obtained up to large values of the wave vector transfer q. It contains many Bragg reflections which may reveal much more structural information than X-rays. In particular, the pair distribution function (PDF) of the nanotubes can be extracted from neutron diffraction data and compared to that of graphite.

X-ray and neutron diffraction profiles of MWNTs often display additional

peaks with smaller intensities than those described above. These peaks correspond to (hkl) reflections of graphite which only exist if some regular stacking of the layers occurs.

2.3 The pair distribution function (PDF)

Neutron diffraction has become a useful tool because intense neutron beams are available from reactors. These neutrons are in thermal equilibrium with the moderator, and their spectrum is approximately Maxwellian, with the temperature of the moderator. At 300 K, the mean energy of the neutrons is about 0.025 eV and their de Broglie wave length is 1.8 Å.

Neutrons interact with the nucleus via the nuclear forces and with the magnetic moment of unpaired electrons via the electromagnetic forces. The magnetic interaction permits the investigation of magnetic materials.

Returning to the problem of the control of the nanotube chirality there is strong evidence supporting the idea that in certain production methods we can obtain a preferred chirality [6, 7] (mainly armchair or zigzag nanotubes are obtained). Methods such as nanodiffraction [6] and high resolution Raman scattering [8, 9] have been used to characterize chirality in individual SWCNTs [10]. In the case of a sample composed mainly of armchair or zigzag nanotubes we need a method which allows us to measure in average what kind of nanotubes are present in our sample, Raman scattering can be used in this case. However, we propose that the pair distribution function (PDF) can be used as a complementary technique.

The PDF allows us to study the local environment of atoms in a small cluster [11], therefore calculating the PDF of a sample of nanotubes we can obtain the arrangement of the atoms by observing the location of the peaks. Certainly, if our sample is composed mainly of nanotubes of one chirality we must observe a distinctive behavior in the PDF.

Because of the sensitivity of this technique, due to the constant structure factor, it becomes a useful tool to study locally dopped semiconductors and alloys, much better than other techniques like extended x-ray absorption fine-structure (XAFS) [11]. The PDF is one way to study the arrangement of atoms in a small cluster and is the spherically averaged distribution of interatomic vector lenghts. In general, the PDF is obtained from the experimental diffraction data by the Fourier transform of the reduced scattering

intensity $S(q)$. Mathematically, it is defined as follows [12, 13]:

$$G(r) = 4\pi [\ \rho(r) - \rho_0\ ] = \frac{2}{\pi r}\int_0^\infty S(q)\sin(qr)dq, \tag{2.1}$$

where $G(r)$ is the PDF, $\rho(r)$ is the density function, which describes the average probability per unit volume of finding an atom at a position r from an atom at the origin; ρ_0 is the average number density of the material [12, 13]. $S(q)$ is calculated as:

$$S(q) = \frac{1}{Nf^2}\sum_m\sum_n \frac{\sin[q(r_m - r_n)]}{q(r_m - r_n)}\exp(-q^2\sigma^2) \tag{2.2}$$

in the last equation N is the number of atoms in the model, r_i is the position of the atom i, $f = 3.0$ e atom^{-1} is the scattering factor of carbon atoms and $\sigma = 0.05$ Å accounts for the atomic thermal motions. From Eq. 2.1 we have the limit $G(r) \to 0$ as $r \to \infty$, because this fact we can obtain the size of a sample. Also, $G(r) \to 0$ when $r \to 0$ because $S(q) \approx 0$ in this case.

2.3.1 Single-walled carbon nanotubes

As discussed earlier, carbon nanotubes exhibit outstanding mechanical and electronic properties. Theoretically, it is possible to construct a carbon tube by rolling up a hexagonal graphene sheet in various ways. Two of these are "non-chiral", so that the honeycomb lattices located at the top and bottom of the tube are always parallel. These configurations are known as armchair and zigzag. In the arm-chair structure, two C-C bonds on opposite sides of each hexagon are perpendicular to the tube axis, whereas in the zigzag arrangement, these bonds are parallel to the tube axis. All other conformations, where the C-C bonds lie at an angle to the tube axis, are known as "chiral" or helical structures (see Fig 2.8). Then, we can have different sets of distances between the C-C bonds in SWCNTs depending on the particular chirality.

2.3.2 Double-walled carbon nanotubes

Double walled nantubes (DWNTs) consist of two concentric cylindrical graphene layers [15]. The selective synthesis of DWNTs have been recently reported, offering an opportunity to further study their structure. The DWNTs can

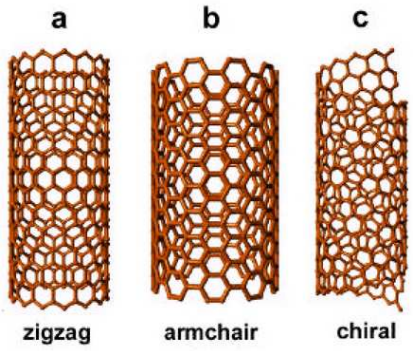

Figure 2.8: Possible kinds of nanotubes obtained by rolling up a graphene sheet. (a) and (b) are non-chiral nanotubes called zigzag and armchair nanotubes, respectively. (c) is a typical chiral nanotube [14].

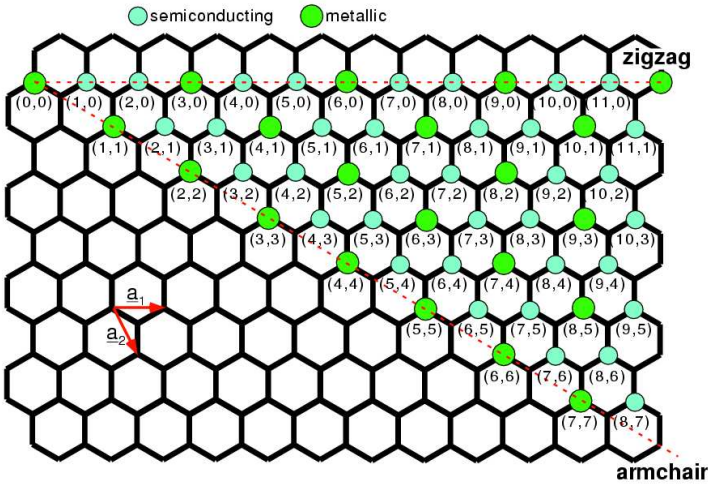

Figure 2.9: Chiral vectors for SWNTs $\vec{a}_1$ and $\vec{a}_2$. The 3-D structure of each nanotube is specified by giving the chiral angle θ and the diameter of the tube. The circles in turquoise and green indicates the key positions to obtain a metallic or semiconducting nanotube.

be synthesized by different methods such as arc discharge [16], coalescence of C_{60} peapods [17], and chemical vapour deposition (CVD) [18]. Depending of these synthesis methods, different values of intertube spacing have been reported.

Recently [15], DWNTs have been produced DWNTs with a high degree of purity wich is very important for technological applications. The distribution of diameters was found by using Raman scattering. It was found that the diameter ratios were 0.77 nm:1.43 nm and 0.9 nm:1.6 nm for the inner tubes and the outer tubes. Also, the bundles of DWNTs are ordered in trigonal arrangements, see Fig. 2.10.

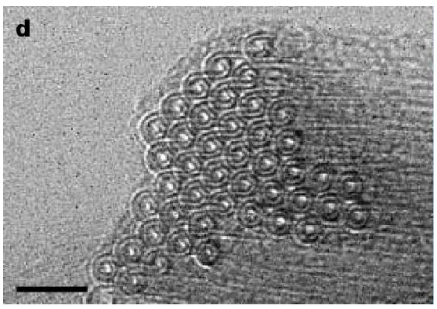

Figure 2.10: HRTEM image of a bundle of DWNTs showing the hexagonal packing structure. Scale bar 5 nm [15].

2.3.3 Fullerenes

Fullerenes are polyhedral carbon structures built up by n three coordinated carbon atoms with 12 pentagons and n hexagons, where the minimum for n equals 20. Fullerenes fullfill Euler's theorem, that states that a polyhedron built up from pentagons and hexagons contains exactly 12 pentagons, to make a closed structure. Following this rule, the dodecahedron with 20 carbon atoms is the smallest possible fullerene. Actually, the smallest and most stable fullerene found is C_{60}, because it is the first fullerene in the series that does not contain adjacent pentagons. If two pentagons are annealed, the tension of the binding increases and the structure is less energetically stable.

Giant classical fullerenes are fullerenes containing 12 pentagons and a large number of hexagons. These structures are stable and therefore it could be possible to synthesize them experimentally. We study giant fullerenes

which have five-fold symmetry permitting only pentagons and hexagons in their structure. This has the effect of faceting the polyhedron. The structure turns out to be more faceted when the value of n is increased [14, 19].

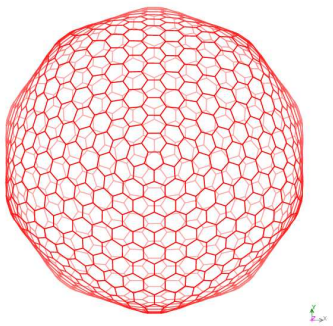

Figure 2.11: Fullerene C_{1500} oriented along the C_5 axis. Notice the faceting, which is due to the pentagonal defects.

2.3.4 Haeckelites

Haeckelites consist of ordered statistically planar arrangements of pentagons, hexagons and heptagons [20]. These structures turn out to be more stable than C_{60}. We study here the following structures:

(1) Rectangular, labeled by R, containing only heptagons and pentagons paired symmetrically within a flat surface. Its generation can be achieved by the creation of Stone-Wales type defects on the graphene sheet, transforming pyrenelike rings into two pairs of heptagons and pentagons.

(2) Hexagonal, labeled by H, which exhibits repetitive units of three agglomerated heptagons surrounded by alternating pentagons and hexagons.

(3) Oblique, labeled by O, containing pentalene and heptalene units bound together and surrounded by six membered rings.

Tubular structures can be constructed from these 2D arrays in exactly the same way as graphene tubules.

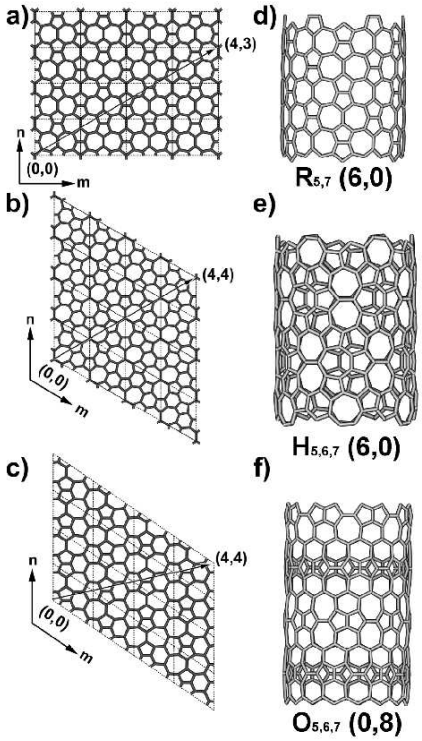

Figure 2.12: Haeckelites structures (a) rectangular cell, (b) hexagonal cell and (c) oblique cell. The way in which these structures are generated is the same as that of SWNTs. The tubes shown are non-chiral with a diameter of approximately 14 Å. (d), (e) and (f) show a R(6,0), H(6,0) and O(0,8) Haeckelite, respectively [20].

Bibliography

[1] *Raman spectroscopy for chemical analysis*, R. L. McCreery, **157** (Wiley 2000).

[2] *Single nanotube raman spectroscopy*, M. S. Dresselhaus, G. Dresselhaus, A. Jorio, A. G. Souza, M. A. Pimenta, and R. Saito, Acc. Chem. Res. **35**, 1070 (2002).

[3] *Structure of carbon nanotubes probed by local and global probes*, Ph. Lambin, A. Loiseau, C. Culot and L. P. Biró, Carbon **40**, 1635 (2002).

[4] *Second-order resonant Raman spectra of single-walled carbon nanotubes*, S. D. M. Brown, P. Corio, A. Marucci, M. A. Pimenta, M. S. Dresselhaus and G. Dresselhaus, Phys. Rev. B **61**, 7734 (2000).

[5] *Helical microtubules of graphitic carbon*, S. Iijima, Nature (London) **354**, 56 (1991).

[6] *Boron-mediated growth of long helicity-selected carbon nanotubes*, X. Blase, J. C. Charlier, A. De Vita, R. Car, Ph. Redlich, M. Terrones, W. K. Hsu, H. Terrones, D. L. Carroll and P. M. Ajayan, Phys. Rev. Lett. **83**, 5078 (1999).

[7] *Crystalline ropes of metallic carbon nanotubes*, A. Thess, R. Lee, P. Nikolaev, H. Dai, P. Petit, J. Robert, C. Xu, Y. H. Lee, S. G. Kim, A. G. Rinzler, D. Colbert, G. Scuseria, D. Tománek, J. E. Fischer and R. Smalley, Science **273**, 483 (1996).

[8] *Chirality-dependent G-band Raman intensity of carbon nanotubes*, R. Saito, A. Jorio, J. H. Hafner, C. M. Lieber, M. Hunter, T. McClure, G. Dresselhaus and M. Dresselhaus, Phys. Rev. B **64**, 085312 (2001).

[9] *Observations of the D-band feature in the Raman spectra of carbon nanotubes*, S. D. M. Brown, A. Jorio, G. Dresselhaus and M. Dresselhaus, Phys. Rev. B **64**, 073403-1 (2001).

[10] *Resonant Raman spectra for isolated single-wall carbon nanotubes grown*, A. Jorio, R. Saito, J. H. Hafner, C. M. Lieber, M. Hunter, T. McClure, G. Dresselhaus and M. Dresselhaus, Phys. Rev. Lett. **86**, 1118 (2001).

[11] *Direct observation of the structure of gold nanoparticles by total scattering powder neutron diffraction*, K. Page, T. Proffen, H. Terrones, M. Terrones, L. Lee, Y. Yang, S. Stemmer, R. Seshadri and A. K. Cheetham, Chem. Phys. Lett. **393**, 385 (2004).

[12] *Local atomic structure of semiconductor alloys using pair distribution functions*, J. S. Chung and M. F. Thorpe, Phys. Rev. B **55**, 1545 (1997).

[13] *Local atomic structure of semiconductor alloys using pair distribution functions. II*, J. S. Chung and M. F. Thorpe, Phys. Rev. B **59**, 4807 (1999).

[14] *Curved nanomaterials*, Terrones, H., Terrones M., and M., Moran-Lopez, J.L., Current Science **81**, 1011 (2001).

[15] *'Buckypaper' from coaxial nanotubes*, M. Endo, H. Muramatsu, T. Hayashi, Y. A. Kim, M. Terrones and M. S. Dresselhaus, Nature (London) **433**, 476 (2005).

[16] *Double-walled carbon nanotubes fabricated by a hydrogen arc discharge method*, J. L. Hutchinson, N. A. Kiselev, E. P. Krinichnaya, A. V. Krestinin, R. O. Loufly, A. P. Morawski, V. E. Muradyan, E. D. Obraztsova, J. Sloan, S. V. Terekhov and D. N. Zakharov, Carbon **39**, 761 (2001).

[17] *Raman scattering study of double-wall carbon nanotubes derived from the chains of fullerenes in single-wall carbon nanotubes*, S. Bandow, M. Takizawa, K. Hirahara, M. Yudasaka and S. Iijima, Chem. Phys. Lett. **337**, 48 (2001).

[18] *Morphology, diameter distribution and Raman scattering measurements of double-walled carbon nanotubes synthesized by catalytic decomposition of methane*, W. Ren, F. Li, J. Chen, S. Bai and H.-M. Cheng, Chem. Phys. Lett. **359**, 196 (2002).

[19] *Structure, chirality, and formation of giant icosahedral fullerenes and spherical graphitic onions*, Terrones, M., Terrones, G., and Terrones H., Structural Chemistry **13**, 373 (2002).

[20] *New metallic allotropes of planar and tubular carbon*, H. Terrones, M. Terrones, E. Hernández, N. Grobert, J-C. Charlier and P. M. Ajayan Phys. Rev. Lett. **84**, 1716 (2000).

[21] *Nobel Lectures, Chemistry 1996-2000*, Ingmar Grenthe, (World Scientific Publishing Co., Singapore, 2003).

[22] *Curved nanostructured materials* Terrones, H., and Terrones M., New Jour. of Phys. **5**, 126.1 (2003).

[23] *Application of atomic pair distribution function analysis to materials with intrinsic disorder. Three-dimensional structure of exfoliated-restacked WS_2 : not just a random turbostratic assembly of layers*, V Petkov, S. J. Billinge, J. Heising and M. G. Kanatzidis, Jour. of the Chem. Soc. **122**, 11571 (2000).

[24] *Characterizing carbon nanotube samples with resonance Raman scattering*, A. Jorio, M. A. Pimenta, A. G. Souza Filho, R. Saito, G. Dresselhaus and M. S. Dresselhaus, New Journal of Physics **5**, 139.1 (2003).

Chapter 3

Some applications of the PDF

Contents

Most of what we know about the geometrical characteristics of carbon nanotubes arises from direct imaging techniques: high resolution transmission electron microscopy, scanning electron microscopy, and atomic force or scanning tunneling microscopy. Such characterisations provide information about the arrangement of atoms within a single nanotube, the determination of diameter, chirality (or helicity), and the number of individual nanotubes in stacking and defects. However, they proved difficult for bulk nanotube systems. Selected area electron diffraction and electron diffraction provided structural nanotube information. The nanotube diameter can be probed by Raman spectroscopy as it is inversely proportional to the frequency of the radial breathing mode. All these techniques are valuable in providing information on specific regions of the volume of the sample and therefore are local probes of the structure. In order to obtain structural details of bulk samples an alternative approach is to use the wide angle X-ray or neutron scattering methods. Relatively little work has been published on the use of these techniques [1, 2, 3, 4] and precise bond lengths, chirality, possible distortions of the hexagonal network are not firmly established. In order to address these structural questions the method of the pair distribution function is applied in the present chapter to study the structure of SWNTs, Haecklites and Fullerenes. Recently, Burian et. al. [5, 6, 7] has calculated the structure factor of single and multiwalled carbon nanotubes finding certain features related to diameter and chirality.

3.1 Experimental observations using neutron diffraction

The neutron data were collected using total scattering powder neutron diffraction on the NPDF diffractometer at the Manuel Lujan Jr. Neutron Scattering Center. The HIPCO samples were sealed in vanadium cans and cooled using a closed cycle refrigerator. The data were corrected for instrument background, incident neutron spectrum, absorption and multiple scattering, and finally normalized using the program PDFgetN [8]. Data up to $Q = 30$ Å^{-1} were used in the Fourier transform, giving a high real space resolution of $\Delta r \sim 0.2$ Å.

3.2 Nanotube characterization

In order to elucidate the behavior of the PDFs of SWCNTs we performed calculations for arm-chair and zig-zag nanotubes using the Cerius program [12]. The input parameters for the first and second gaussian broadening were taken to coincide with those of Ref. [9]; the values are $\sigma_1 = 0.1$ and $\sigma_2 = 0.8$. Chiral nanotubes do not have a common pattern for C-C lengths like armchair and zigzag nanotubes and also have long unit cells. However, we believe that using the PDF to make a data base we can recognize the chirality of each nanotube. Chiral nanotubes will be fully studied in the future.

A typical PDF pattern allows us to observe the most common distances in specific arrangement of atoms in a sensitive way. For example, in Ref.[9] the authors studied the differences between surface and bulk distances for Au clusters using this technique. Also, the PDF provides information about the size of the sample.

As it was mentioned above for SWNTs, we have different sets of distances between C-C bonds because of their different chiralities. Therefore, at first glance it seems that the PDFs can be used as a fingerprint to probe each nanotube.

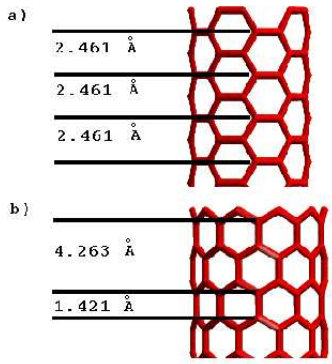

Figure 3.1: Nanotubes with zero chirality have characteristic distances that are not found in other chiral nanotubes. In a) and b) we show those distances for armchair and zigzag nanotubes. For armchair nanotubes these distances are multiples of 2.462 Å, while for zigzag nanotubes are multiples of 4.263 Å.

3.2.1 Armchair and zigzag nanotubes

In general, we found that the PDF pattern gives valuable information when we consider a short range of distances, $0 < r < 11$ Å. For greater distances the signal becomes irregular. We analyzed only short ranges ($0 < r < 15$ Å) of the PDF patterns. In this interval of distances, the armchair and zigzag nanotubes exhibit distinctive distances between C-C atoms as shown in Fig. 3.1.

As we will see later, in general we can find the smallest distances between carbon atoms for carbon structures (SWNT, fullerene, Haeckelite, etc.) with a very good precision by using the PDF. For example Fig. 3.2 shows typical distances between C-C atoms for pentagon, hexagons and heptagons commonly found in structures containing them. It is important to notice that the appearence of such distances will depend mainly on two factors. First, it comes the resolution of the diffractometer. By using high resolution, it would be possible to observe very small distances and to detect small differences between two close distances. The second is the concentration of those geometrical defects in the sample. This fact permits to consider the PDF as a technique useful to distinguish many types of defects, such as kinks, Stone-Wales, etc.

As we show in Fig. 3.1, for armchair nanotubes the characteristic distances are multiples of 2.462 Å and for zigzag are multiples of 4.263 Å. Obviuosly, in the case of chiral nanotubes we cannot find a general rule like that for amrchair and zigzag. Instead, it depends on the diameter and the chiral angle. In Figs. 3.3 and 3.4 we present the first two characteristic peaks in the PDF for armchair and zigzag nanotubes correspondig to 2.462 Å, 4.924 Å and 4.263 Å, 8.526 Å, respectively (the first and second broadening in this were $\sigma_1 = 0.009$ and $\sigma_2 = 0.8$). In the case of carbon nanotubes made only with hexagons and heptagons, we expect that the characteristic peaks related to heptagons do not appear in the PDF. In the same way, when we study the PDF for Haeckelites structures [10], we expect peaks shown in Fig. 3.2. Certainly, the magnitude of such peaks will depend on the concentration of the defects.

We calculated the PDFs for SWNTs without cap, armchair and zigzag, with diameters between $4-27$ Å as we show in Table B.1 and B.2 in appendix B. The lengths of the studied nanotubes were approximately 130 Å, the number of carbon atoms for each nanotube was 1200. These range of diameters is usually found in experiments carried on by techniques such as chemical vapor deposition and laser ablation [1, 3]. Figs. 3.5 and 3.6 show the PDFs

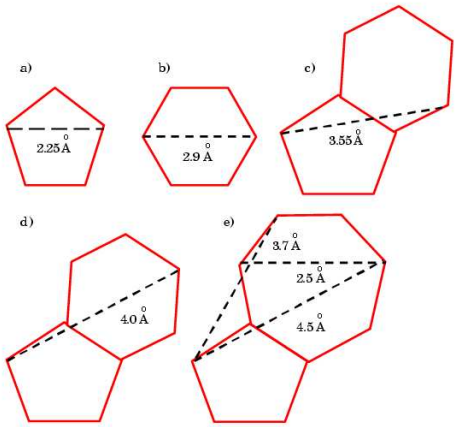

Figure 3.2: Some typical distances found in the PDF for the case of a sample containing geometrical defects, such as pentagons, hexagons and heptagons. The observation of these distances depends on the resolution of the device and the concentration of the defects.

for armchair and zigzag nanotubes. We notice that when distance r is small ($r < 6$ Å), the set of distances are equal to those found in a graphene layer, as we expect, because for C-C neighbors the distances are slightly distorted with respect to a planar lattice of graphene; see for example the 1.421 Å (the distance between C-C bonds to first neighbors) and 2.461A Å (the distance between C-C bonds to second neighbors). For $r > 6$ Å, the PDFs are different from each other because of the possible arrays of distances between carbon atoms. Therefore, we identify this interval, $r > 6$ Å, as that where the PDFs can be used to distinguish nanotube chiralities. The behavior of the PDFs for different armchair nanotubes is more similar to the PDF of the graphene layer in the range $0 < r < 8$ Å than those of zigzag nanotubes. This fact is because for armchair nanotubes the distances to first neighbors are slightly modified in the process of wrapping of the graphite sheet to form the nanotube. In general, for any diameter, the armchair and zigzag nanotubes follow a pattern like that shown in Figs. 3.5 and 3.6. These patterns can be used to characterize those tubes with zero chirality. The inset of Figs. 3.5 and 3.6 also shows that besides the characteristic distances for armchair nanotubes mentioned above, there exist the common distances at $r = 5.1$ Å and $r = 5.68$ Å which are not present in zigzag nanotubes. This fact permits to distinguish between armchair and zigzag nanotubes.

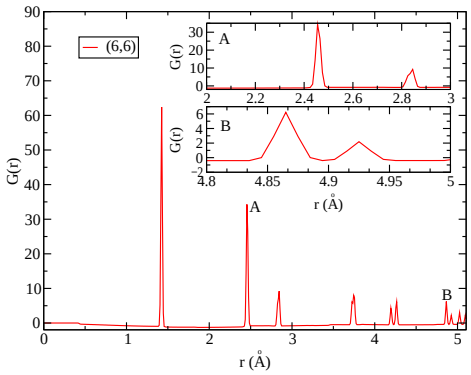

Figure 3.3: The first two typical peaks of (6,6) armchair nanotubes, A = 2.46 Å and B = 4.92 Å.

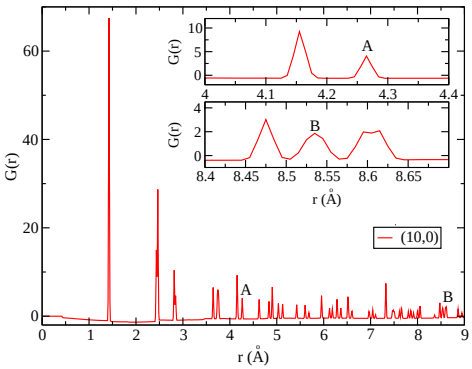

Figure 3.4: The first two typical peaks of (10,0) zigzag nanotubes, A = 4.26 Å and B = 8.53 Å.

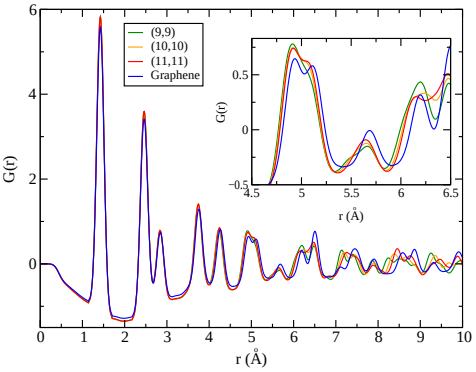

Figure 3.5: The armchair nanotubes show a disordered pattern beyond 8 Å. Observe the great coincidence in this range with the PDF of a graphene layer.

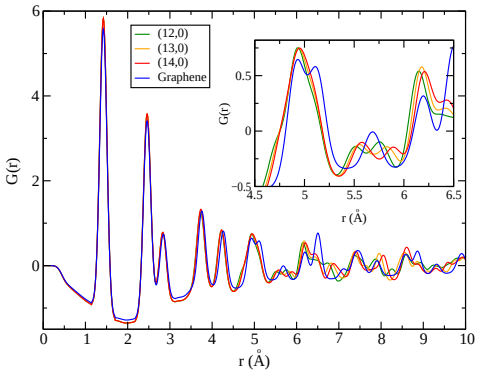

Figure 3.6: The zigzag nanotubes present an ordered behavior as in the case for armchair nantubes in the range 8 Å. The PDF for armchair is different from the graphene one beyond 5 Å.

The effect of the diameters of the nanotubes is shown in Fig. 3.7. We compared three PDFs for small, intermediate and big diameters of nanotubes with the PDF of a graphene layer. The PDF of a (20,20) nanotube and that of the graphene layer is more similar than that of (3,3) and (10,10) nanotubes, this is because (20,20) nanotube is more planar than (3,3) and (10,10) nanotubes, i.e. its curvature is smaller.

We know that the tubes in a sample are arrayed in bundles and also that this bundles are hexagonally packed [1, 11]. We calculated the PDF for a trigonal cell of (10,10) nanotubes with lattice parameter equal to 17 Å and intertube separation equal to 3.4 Å. The results are shown in Fig. 3.8. The PDFs in this case are very similar in the interval $0 < r < 15$ Å. Beyond this range the position of the peaks coincides even though the intensities of the peaks are higher in the case of the PDF for the trigonal cell, this is because distances bigger than 15 Å involve C-C distances between different nanotubes, the diameter of the (10,10) nanotube is 14.7 Å.

3.2.2 Comparison with experimental PDF

We compared the theoretical PDFs for armchair nanotubes and zigzag nanotubes with the experimental one obtained from a HIPCO sample. We found coincidences for armchair and zigzag nanotubes signals with the experimental signal. However, the coincidence was not complete: there were certain peaks which could not be explained by the presence of any armchair or zigzag

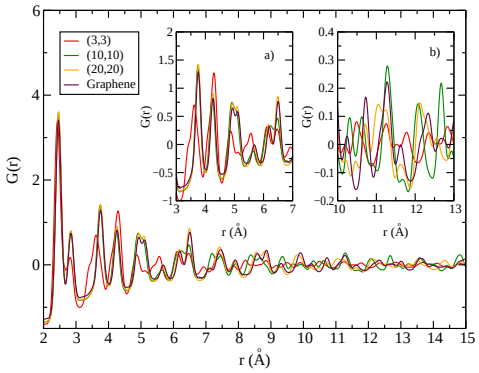

Figure 3.7: The effect of the diameter in the PDF is shown for three armchair nanotubes with small, intermediate and big diameters (3,3), (10,10) and (20,20) respectively. These PDFs are compared with the PDF of a graphene layer. As the diameter increases, the PDF of the nanotubes is more similar to the PDF of the graphene. In the inset figures a) and b) we show the last fact. Also a) indicates that for distances $r > 7$ Å, the PDFs of the nanotubes becomes different from that of the graphene. This is due to the effect of curvature. However, for bigger tubes we expect this tendency to disapear (see appendix B for diameters).

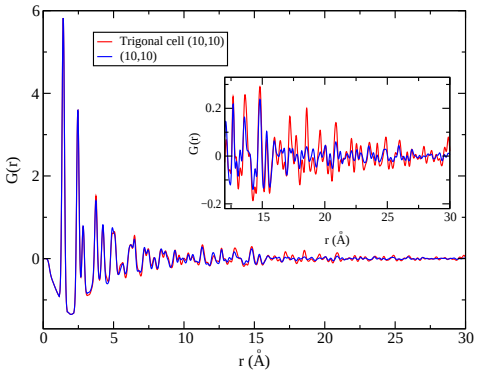

Figure 3.8: The PDF permits to observe the effect of the arrays of nanotubes in bundles. We calculated the PDF of a single (10,10) nanotube and compared it with the PDF of a trigonal cell of (10,10) nanotubes with lattice parameters equal to 17 Å and intertube separation equal to 3.4 Å. The PDFs of both the cell and the single tube are similar for distances $r < 15$ Å [diameter of the (10,10) nanotube], but they are different for bigger distances as we show in the inset figure. We can infer that the amplitudes of the PDF gives information about the size of the sample. It is clear that for little samples we do not expect the amplitudes to be different from those of the graphene layer.

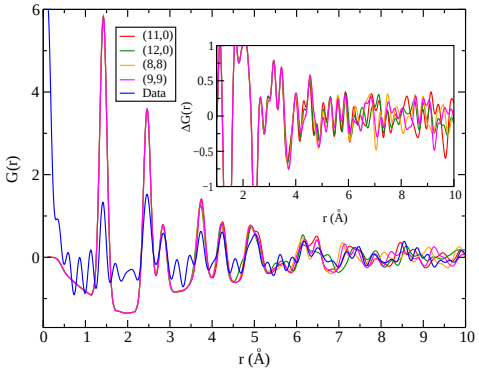

Figure 3.9: When we compare the typical distances in armchair and zigzag nanotubes with the experiment we found that the PDFs coincide in range $r < 8$ Å in both cases, except for the peaks in $r = 1.7$ Å, 2.0 Å, 3.2 Å, 3.5 Å, 4.5 Å, 5.3 Å, and 5.9 Å. In the inset figure we show the difference graph between the experimental PDF and the theoretical ones. As we can see the differences are of the same magnitude and we cannot conclude anything about a preferred chirality in the sample.

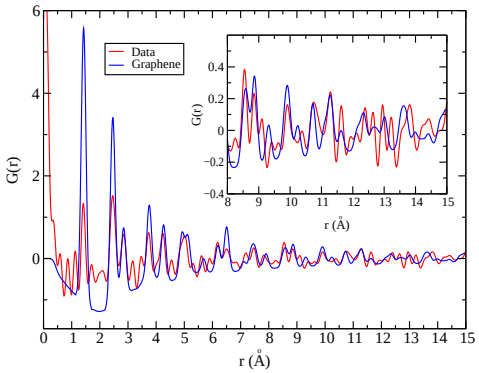

Figure 3.10: The experimental PDF shows good agreement with the PDF of the graphene for distances up to $r = 11$ Å. This fact shows that the sample could contain nanotubes with diameters bigger than 11 Å, because the experimental PDF is slightly modified by effects of curvature in the interval mentioned.

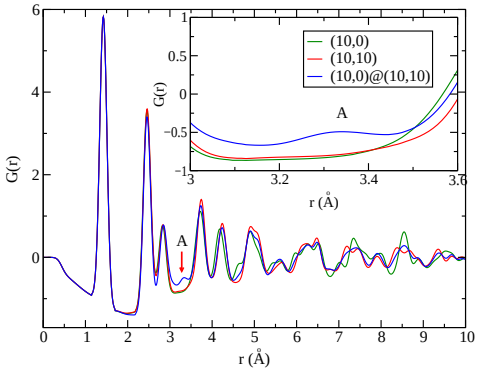

Figure 3.11: The PDF of DWNTs presents features related to the intratube spacing, the peak labeled as $A = 3.4$ Å in the figure denotes this fact. The PDF of the DWNT (10,0)@(10,10) is compared with that of the (10,10) and (10,0) nanotubes. The PDF of the DWNT includes features of the (10,10) and (10,0). However, we notice that the PDF of the DWNT is more similar to that of (10,10) nanotube, this is due to the fact that (10,10) nanotube is bigger than (10,0) nanotube and we expect a higher amount of C-C bonds in that tube.

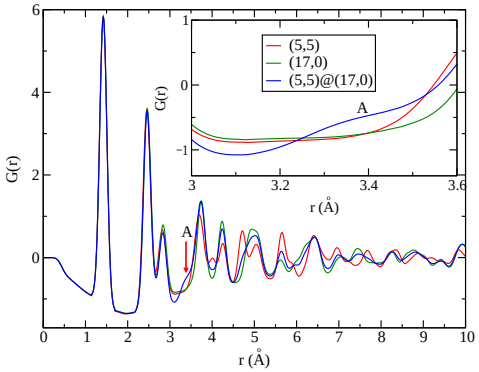

Figure 3.12: As in Fig. 3.11 we can observe the intratube separation $A = 3.4$ Å. Also the experimental PDF is more similar to that of the PDF of the bigest tube.

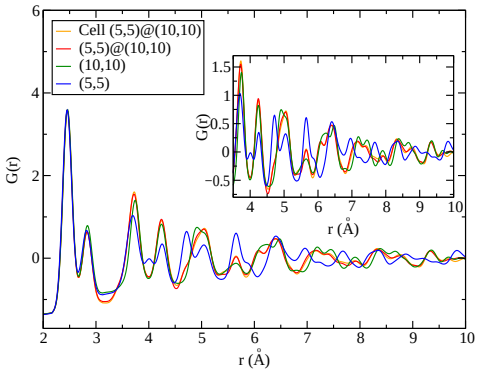

Figure 3.13: We calculated the PDF for a trigonal cell of (10,0)@(10,10) nanotubes and a single (10,0)@(10,10). The PDFs of both cell of nanotubes and single nanotube are slightly modified up to $r = 10$ Å. The PDFs of (10,10) and (5,5) nanotubes are shown in the same graph just for comparison and to observe the effect of the diameter.

nanotube. Also, the differences between the experimental PDF and the theoretical ones lies in the same orden of magnitude and we cannot conclude anything about a preferred chirality in the sample. This is shown in Fig. 3.9. The differences can be atributed to the small size of the sample, then the experimental PDF is corrected from small size effect with theoretical models [13, 14] which are approximated. Also, the theoretical PDFs consider perfect nanotubes without geometrical defects, but the real nanotubes are imperfect. The impurities can introduce an extra component in the PDF not considered in the Cerius2 software used to calculate the PDFs. Also Cerius2 software takes into account the effect of the size and small angle by the Mitchell model [13] and this model is an approximation of the reality.

The experimental PDF (see Fig. 3.10) shows good agreement with the PDF of a graphene layer for distances below 11 Å. This is explained by the presence of mainly nanotubes with big diameter, because for those nanotubes the PDF is slightly modified respect the graphene one.

3.2.3 Double-walled carbon nanotubes

The PDFs for DWNTs show features appearing in their constitutent parts, but also permit to obtain the intratube separation and the chirality of the biggest tube. The smallest tube distances are absorbed by the biggest tube and in average their contribution to PDF is neglected if the sample is small, see Figs. 3.11 and 3.12.

The PDF for a trigonal cell of (5,5)@(10,10) nanotubes presented in Fig. 3.14 is very close to the PDF of a single (5,5)@(10,10). However, our cells contained only 36 nanotubes, and this result could be modified if we increase the number of nanotubes in the cell, this is shown in, see 3.13.

3.3 Fullerene characterization

Fullerenes are spherical structures made of sp^2 carbon atoms. Fullerenes fullfill Euler's rule (see appendix B). If we impose the restriction of having a fivefold symmetry axis, we expect the fullerene to be faceted when the number of atoms is increased. This flattening can be observed in the PDF for fullerenes with different number of atoms as a shift in the peaks, because the curvature radius at the pentagons is increased.

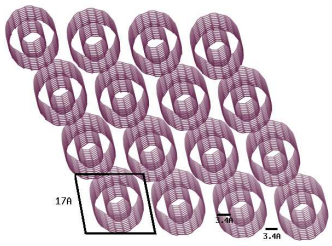

Figure 3.14: Trigonal cell of (5,5)@(10,10) DWNTs. The unit trigonal cell considered contains a single (5,5)@(10,10), the lattice parameter is equal to 17 Å and the intratube and intertube separation is equal to 3.4 Å in both cases, in agreement with recent experiments to produce highly pure samples [11].

This feature shows up in all the peaks, for example the peak at 2.41 Å expected for C-C bonds in C_{60} is displaced in bigger fullerenes; the same is true for the peaks at 2.8 Å and 3.5 Å, as shown in Fig. 3.15. The size of C_{60} is obtained from the PDF and it is stimated in 7.2 Å, the real diameter is approximately 7 Å[15].

Remember that the PDF gives information about the size of the nanostructure and translate to mathematical formalism about the curvature. Also, the intensities of the peaks increase with the number of atoms. These two facts permit obtain information about the concentration of hexagons, in other words the presence of impurities in a certain array of atoms.

The symmetry of the structure can be treated by the PDF as Fig. 3.16 where we have calculated the PDF for two isomers of the C_{80} fullerene having the Ih and D5d symmetry. The size of C_{80} D5d is 8.8 Å and for C_{80} Ih is 8.5 Å as shown in Fig. 3.16, this is explained because the C_{80} D5d has a tubular form and is longer than C_{80} Ih.

3.4 Haeckelite characterization

As we can see in Fig. 2.12, nanotubes can be generated incorporating pentagons, hexagons and heptagons to a graphene sheet. In particular, in this work we consider only three types of them, the Rectangular, Hexagonal and Oblique Haeckelites. The diameters of the Haeckelites we studied are shown in B.3 in appendix B. Rectangular Haeckelites possess pentagonal and hep-

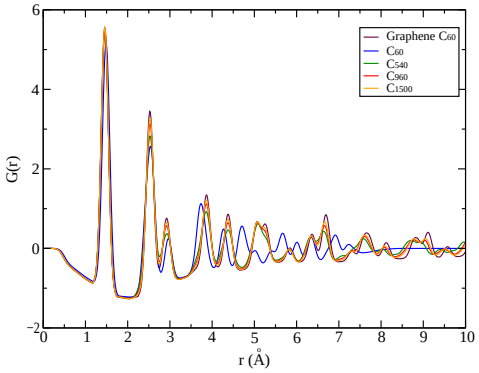

Figure 3.15: Shifting of the peaks for fullerenes as the number of atoms in the structure is increased. As the number of atoms is increased the fullerenes with Ih symmetry tend to be faceted. This originates the fullerene to be faceted and in consequence the PDF for giant fullerenes will be very close to that of a graphene layer.

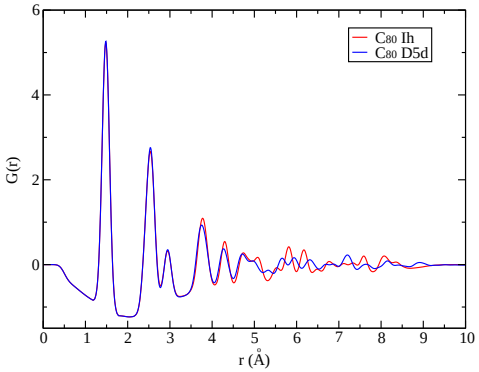

Figure 3.16: PDFs for C_{80} with Ih and D5d symmetry. This fugure shows that the PDF is sensitive to the symmetry of an agregate of atoms. The PDF is practically the same for distances $r < 5$ Å. Beyond this range the PDF can be used to distinguish the symmetry of the C_{80}.

tagonal rings, hexagonal and oblique Haeckelites posess pentagonal, hexagonal and heptagonal rings but in different arrangements. Then we expect different peaks in a PDF pattern as in the case of simple SWNTs.

Because of the presence of pentagons and heptagons in these cylindrical carbon structures, we have characteristic distances to first neighbors (see Fig. 3.2). Other distances can be found, but we focus only on the mentioned ones because of their high intensity, that makes them more probable.

Fig. 3.17 shows the characteristic peaks for hexagonal Haeckelites structure. The peak at 2.5 Å is typical of pentagons, the peak at 2.8 Å and the peaks at 2.5 Å, 3.7 Å, and 4.5 Å are typical of pentagonal-heptagonal adjacencies.

If we compare the PDF of a pure hexagonal SWNT with a rectangular, hexagonal or oblique Haeckelite we would expect the peaks related to heptagons not to appear in the PDF of the simple tube. Also, the peak related to hexagons at 2.8 Å should be missing. This is what we found in Fig. 3.18.

The rectangular Heackelites do not show the peak at 2.8 Å, which is characteristic of hexagons because there are no hexagons in these Haeckelites. Instead we have the pronounced peak at 3.3 Å and 3.7 Å belonging to heptagons. Because the rectangular Haeckelites do not contain hexagons we

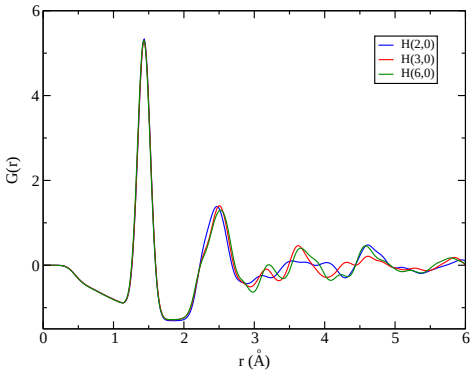

Figure 3.17: Theoretical PDF of three hexagonal Haeckelites of the type (6,0), (3,0) and (2,0). We found the typical distances shown in Fig. 3.2.

can distinguish them with respect to the hexagonal and oblique Haeckelites. This fact is shown in Fig. 3.20. The peaks for hexagons (for example at 2.8 Å) appear for hexagonal and oblique Haeckelites while not for rectangular Haeckelites. For oblique Haeckelites we expect the same peaks that appear in hexagonal Haeckelites. The PDF for a (0,7) oblique Haeckelite is presented in

Fig. 3.21. Also, we observe the signal of oblique Haeckelites be well behaved in the sense that it has the same peaks in the interval of distances that we take into account.

Oblique and hexagonal Haeckelites have the same defects, but they are arranged in a different way, and they have also a different concentration of hexagons. This can be seen in Fig. 3.22, where we compare these two Haeckelite tubes.We notice the peak at 2.9 Å is more prominent in oblique Haeckelite and also shifted with respect to the value for a hexagonal Haeckelite. This shows that the PDF are very sensitive to lattice distortions.

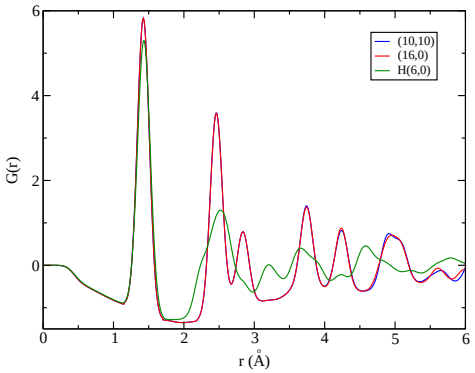

Figure 3.18: Comparison of the theoretical PDF of (10,10) and (16,0) nanotubes and the PDF of the (6,0) hexagonal Haeckelite. We notice that the peak at 2.8 Å characteristic of hexagons is more intense in the PDF of the simple tubes while the peaks in 3.5 Å related to heptagonal-pentagonal defects does not appear in the plot for simple tubes. All the tubes have the same diameter 13.0 Å.

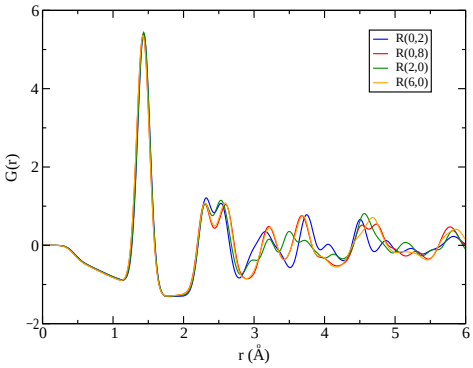

Figure 3.19: Theoretical PDF for four rectangular Haeckelites, (6,0), (2,0), (0,8) and (0,2). The graphs do not show the typical peak of hexagons at 2.8 Å, as it is expected.

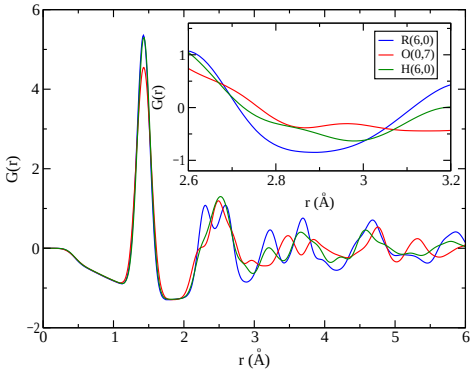

Figure 3.20: Comparison of a (0,7) oblique Haeckelite, a rectangular (6,0) Haeckelite and a hexagonal (6,0) Haeckelite. We can distinguish between them, because the peaks characteristic to hexagons are not present in the rectangular structure.

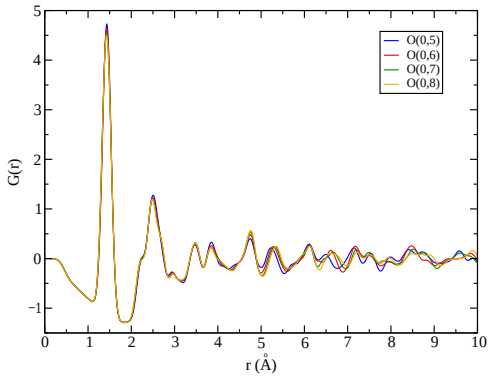

Figure 3.21: Oblique Haeckelites showing a regular behavior.

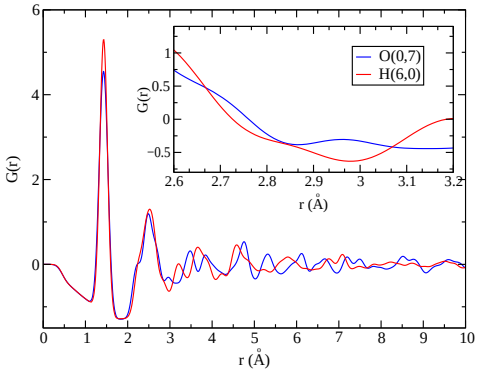

Figure 3.22: Comparison of oblique (0,7) Haeckelite with a hexagonal (6,0) Haeckelite. The peak at 2.8 Å is shifted for the oblique Haeckelite and more intense, revealing some information about the concentration of hexagons in the structure.

Bibliography

[1] *Crystalline ropes of metallic carbon nanotubes*, A. Thess, R. Lee, P. Nikolaev, H. Dai, P. Petit, J. Robert, C. Xu, Y. H. Lee, S. G. Kim, A. G. Rinzler, D. Colbert, G. Scuseria, D. Tománek, J. E. Fischer and R. Smalley, Science **273**, 483 (1996).

[2] *Application of atomic pair distribution function analysis to materials with intrinsic disorder. Three-dimensional structure of exfoliated-restacked WS_2 : not just a random turbostratic assembly of layers*, V Petkov, S. J. Billinge, J. Heising and M. G. Kanatzidis, Jour. of the Chem. Soc. **122**, 11571 (2000).

[3] *Boron-mediated growth of long helicity-selected carbon nanotubes*, X. Blase, J. C. Charlier, A. De Vita, R. Car, Ph. Redlich, M. Terrones, W. K. Hsu, H. Terrones, D. L. Carroll, and P. M. Ajayan, Phys. Rev. Lett. **83**, 5078 (1999).

[4] *Structure of carbon nanotubes probed by local and global probes*, Ph. Lambin, A. Loiseau, C. Culot and L. P. Biró, Carbon **40**, 1635 (2002).

[5] *Radial distribution function analysis of spatial atomic correlations in carbon nanotubes*, Burian A., Koloczek J., Dore J., Hannon A., Nagy J., and Fonseca A., Diam. Rel. Mat. **13**, 1261 (2004).

[6] *Characterization of spatial correlations in carbon nanotubes-modelling*, Koloczek J., Kwon Y., and Burian A., J. Alloy. Comp. **328**, 222 (2001).

[7] *Model-based computation of powder diffraction patterns for carbon nanotubes*, Koloczek J., Burian A., Dore J., and Hannon A., Diam. Rel. Mat. **13**, 1218 (2004).

[8] *PDFgetN: a user-friendly program to extract the total scattering structure factor and the pair distribution function from neutron powder diffraction data*, P. F. Peterson, M. Gutmann, Th. Proffen, S. J. Bilinge, J. Appl. Cryst. **33**, 1192 (2000).

[9] *Direct observation of the structure of gold nanoparticles by total scattering powder neutron diffraction*, K. Page, T. Proffen, H. Terrones, M. Terrones, L. Lee, Y. Yang, S. Stemmer, R. Seshadri and A. K. Cheetham, Chem. Phys. Lett. **393**, 385 (2004).

[10] *New metallic allotropes of planar and tubular carbon*, H. Terrones, M. Terrones, E. Hernández, N. Grobert, J-C. Charlier and P. M. Ajayan Phys. Rev. Lett. **84**, 1716 (2000).

[11] *'Buckypaper' from coaxial nanotubes*, M. Endo, H. Muramatsu, T. Hayashi, Y. A. Kim, M. Terrones and M. S. Dresselhaus, Nature (London) **433**, 476 (2005).

[12] *Cerius^2 program*, Copyright ©2001, Accelrys Inc., a subsidiary of Pharmacopeia Inc.

[13] *Eliminating the small-angle component of the scattering calculated for models*, Mitchell G., Acta Cryst. A**37** , 488 (1981).

[14] *Aprofile refinment method for nuclear and magnetic structures*, Rietveld H., J. Appl. Cryst. **2**, 65 (1969).

[15] *C60: Buckminsterfullerene*, H. W. Kroto, J. R. Heath, S. C. O'Brien, R. F Curl and R. E. Smalley, Nature (London) **318**, 162, (1985).

[16] *Influence of the integration limits on the shape of pair correlation functions of non-crystalline materials*, Hoyer W., Kaban I., and Halm T. J. Opt. Adv. Mat. **3**, 255, (2001).

[17] *Extreme superheating and supercooling of encapsulated metals in fullerenelike shells*, Banhart F., Hernández E., and Terrones M. Phys. Rev. Lett. **90**, 185502, (2003).

[18] *Carbon nanotubes: Synthesis, Structure, Properties and Applications* , Dresselhaus, M. S., G. Dresselhaus and Ph. Avouris, (Springer-Verlag Heidelberg, Germany).

[19] *High energy, high resolution, x-ray studies of the structure of complex materials*, Billinge S. and Petkov V., Report of Dept. Phys. and Ast., Michigan State University.

Chapter 4

Conclusions and future work

We have found that the PDF constitutes a novel technique that can be used to determine nanotube chiralities and we have shown in this work that we can distinguish between armchair and zigzag nanotubes. Also, we open the problem of finding a general method to characterize the structure of any chirality in nanotubes using PDFs.

There are many questions unsolved about the usage of the PDFs to characterize nanostructures. In principle we need to find a general algorithm to characterize any nanotube chirality. In this work we have only considered armchair and zigzag nanotubes. Also we need to take more experimental data to compare with the theoretical ones.

The main aim of this work is to use the PDF to characterize samples with an induced chirality. Our HIPCO sample demonstrated not to have a preferred chirality. Then, we need to produced samples, and to prove with complementary techniques such as STM and Raman spectroscopy to decide if the sample has a preferred chirality and if this coincide with the information provided by the PDF.

Up to now Haeckelites and giant fullerenes have not yet been synthesized. Giant fullerenes can be found in the form of nested fullerenes called onions [1, 2]. We can recognize between rectangular, oblique and hexagonal Haeckelites but we cannot recognize particular chiralities. In the case of fullerenes the PDFs are very similar when we increase the number of carbon atoms.

At the resolution we used, we found characteristic peaks for armchair and zigzag SWNTs and also for Haeckelites, our findings are summarize in Tables 4.1 and 4.2. However, as we mentioned above, increasing or decreasing the resolution of the diffractometer we can observe more or less peaks in the PDF

Armchair nanotubes (Å)	Zigzag nanotubes (Å)
1.42	1.42
2.46	4.26
4.92	7.10
7.38	8.52
9.84	11.36

Table 4.1: Typical distances for armchair and zigzag nanotubes to first neighbors.

Rectangular (Å)	Hexagonal (Å)	Oblique (Å)
1.42	1.42	1.42
2.25	2.25	2.25
2.50	2.50	2.50
3.70	2.90	2.90
4.50	3.55	3.55
-	3.70	3.70
-	4.00	4.00
-	4.50	4.50

Table 4.2: Typical distances for Haeckelites to first neighbors. Observe that rectangular Haeckelites do not posses the features related to the presence of hexagonal rings.

pattern. In the limit of a Dirac delta PDF pattern, we would observe all the distances between atoms in the structure, this is based in Fig. 3.2.

The technique of the PDF can be used for other nanostructures can be used to study other nanostructures such as encapculated C_{60} [3], nanotubos dopados con boro [4], nanopeapods [5], etc.

Bibliography

[1] *Curling and closure of graphitic networks under electron beam irradiation*, Ugarte D., Nature **359**, 707 (1992).

[2] *Structure, chirality, and formation of giant icosahedral fullerenes and spherical graphitic onions, structural*, Terrones, M., Terrones, G., and Terrones, H., Chem. **13**, 513 2002.

[3] *Encapsulated C_{60} in carbon nanotubes*, Smith B., Monthioux M., and Luzzi D., Nature, **396**, 324 1998.

[4] *Boron-doping effects in carbon nanotubes*, Wen K., Firth S., Redlich P., Terrones M., Terrones H., Zhu Y., Grobert N., SchilderA., Clark R., Kroto H., and Walton D., J. Mater. Chem., **10**, 1425 2000.

[5] *Fullerene coalescence in nanopeapods: a path to novel tubular carbon*, Hernández E., Meunier V., Smith B., Rurali R., Terrones H., Nardelli B., Terrones M., Luzzi D., and Charlier J., Nanoletters, **0**, 5 2003.

[6] *Carbon nanotubes: Synthesis, Structure, Properties and Applications* , Dresselhaus, M. S., G. Dresselhaus and Ph. Avouris, (Springer-Verlag Heidelberg, Germany).

Appendix A

Chiral vectors of carbon nanotubes

A.1 Single-walled carbon nanotubes

All of the chiralities of nanotubes can be obtained by specifying two integer numbers in the form (n, m) denoting the length of two lattice vectors needed to roll-up the graphite sheet. The lattice vectors are named chiral vectors $\vec{a}_1$ and $\vec{a}_2$.

The chiral vector is defined as $\vec{C}_h = n\vec{a}_1 + m\vec{a}_2$ with n and m integers and $\vec{a}_1$ and $\vec{a}_2$ the lattice vectors for a hexagonal lattice. The lattice vectors can be expressed in cartesian coordinates as,

$$\vec{a}_1 = \left(\frac{3}{2}a_{cc}, \frac{\sqrt{3}}{2}a_{cc}\right), \vec{a}_2 = \left(\frac{3}{2}a_{cc}, -\frac{\sqrt{3}}{2}a_{cc}\right), \tag{A.1}$$

where a_{cc} is the bond length of carbon atoms and it is equal to $a_{cc} = 1.44A$ for nanotubes.

The length of the chiral vector C_h is the peripheral length of the nanotube:

$$C_h = \sqrt{3}a_{cc}\sqrt{n^2 + nm + m^2}. \tag{A.2}$$

Special cases:

- Armchair nanotube (m=n): $C_h = 3na_{cc}$
- Zigzag nanotube (m=0): $C_h = \sqrt{3}na_{cc}$

The diameter of the nanotube, d_t, is defined as:

$$d_t = \frac{C_h}{\pi} = \frac{\sqrt{3}a_{cc}}{\pi}\sqrt{n^2 + nm + m^2}. \tag{A.3}$$

Special cases:

- Armchair nanotube (m=n): $d_t = \frac{3n}{\pi}a_{cc}$
- Zigzag nanotube (m=0): $d_t = \frac{\sqrt{3}n}{\pi}a_{cc}$

The unit lattice vector (translational vector) T, perpendicular to the chiral vector is expressed as:

$$T = \frac{(2m+n)a_1 - (2n+m)a_2}{d_R}, \tag{A.4}$$

where $d_R = d$ if $n - m$ is not a multiple of $3d$ and $d_R = 3d$ if $n - m$ is a multiple of $3d$, d is the highest common divisor of (n,m).

The chiral angle θ (between the chiral vector and the zigzag direction) is defined as:

$$\theta = \tan^{-1}\frac{\sqrt{3}m}{m+2n}. \tag{A.5}$$

Special cases:

- Armchair nanotube (m=n): $\theta = \tan^{-1}\frac{1}{\sqrt{3}} = 30^o$
- Zigzag nanotube (m=0): $\theta = \tan^{-1} 0 = 0^o$
- Chiral nanotube: $0 < \theta < 30^o$

By choosing a certain chiral angle we can construct a particular nanotube, then depending on the chiral angle we could have different arrays of carbon atoms in nanotubes.

A.2 Haeckelites

For Haeckelites the determination of the n and m indices is different than for SWNTs. In this case we need to build up a unit cell, then n and m are chosen to be the number of unit cells along the axis defined by the cell needed to wrapp of the tube in a certain direction, see 2.12.

Appendix B

Diameters of carbon nanotubes

Armchair SWNTs	Diameter (A°)
(3,3)	4.13
(4,4)	5.47
(5,5)	6.82
(6,6)	8.17
(7,7)	9.52
(8,8)	10.87
(9,9)	12.23
(10,10)	13.58
(11,11)	14.94
(12,12)	16.29
(13,13)	17.65
(14,14)	19.01
(15,15)	20.36
(16,16)	21.72
(20,20)	27.14

Table B.1: Diameters of armchair nanotubes.

zigzag SWNTs	Diameter (A°)
(7,0)	5.53
(8,0)	6.30
(9,0)	7.08
(10,0)	7.86
(11,0)	8.64
(12,0)	9.42
(13,0)	10.02
(14,0)	10.99
(15,0)	11.77
(16,0)	12.55
(17,0)	13.33
(18,0)	14.11
(19,0)	14.90
(20,0)	15.68

Table B.2: Diameters of zigzag nanotubes.

Haeckelite	Diameter ($A°$)
R(0,4)	7.5
R(0,6)	12.0
R(0,8)	14.9
R(4,0)	9.5
R(6,0)	14.2
H(4,0)	9.0
H(6,0)	13.5
O(0,4)	7.1
O(0,6)	10.5

Table B.3: Diameters of Haeckelites.